New Sensing Application to Diagnose Power Semiconductor Aging in Actuator Power Drive Systems

Irfan N. Ali, Antonio E. Ginart, Jonathan W. Goldin, Patrick W. Kalgren, Michael J. Roemer
Impact Technologies
200 Canal View Blvd
Rochester, NY 14623
585-424-1990
Irfan.Ali@impact-tek.com

Scott Poll
NASA Ames Research Center
Moffett Field, CA, 94035, USA
Scott.Poll @nasa.gov

Abstract—**This paper presents a new sensing application to diagnose power semiconductor aging in power drive systems. It has been shown previously that device parasitic characteristics change during the aging process which results in detectable changes in their frequency response. This change is manifested in the current signal at very high frequencies. Therefore, using a wideband AC current sensor, high frequency components of the current can be acquired, providing a way to detect device aging.**

TABLE OF CONTENTS

1. INTRODUCTION

Power electronic converters, drives, and modern electric machines play an increasingly important role in the performance and overall operation of ships, aircraft, space vehicles, ground vehicles and industrial machines. In these applications, maintainability or extended operation is highly desirable during critical operation. Standard power drives found in industry and military settings are based on a power electronics controller and an induction or synchronous Permanent Magnet (PM) motor. The operating frequency band of a standard power drive can be divided in three ranges. The low frequency range, usually below 200 Hz, provides the main electrical signal for the motor and achieves the main purpose of the power drive. The second range, between 10 KHz and 200 KHz in the Pulse Width Modulation (PWM) signal, is used to modulate the main or fundamental signal of the power drive. The third band corresponds to frequencies greater than 1 MHz and is the consequence of the system's resonance and the step functions that formed the PWM signal. This high frequency band is of main interest for modeling and diagnosing transistor aging. Recently high frequency "ringing characterization" has been proposed as an effective method to evaluate aging in transistors. Previous work had been performed on a simplified platform in order to cope with the high complexity of the characterization of the full system. This work deals with the challenges to determine the characteristic frequencies in a full power drive system incorporating a wideband differential AC current sensor. The step inputs introduced by the PWM waveform in a power drive system elicit a response in the system. The system's response at high frequencies establishes the ringing. Exploring use of wideband differential AC current sensors, this paper studies the feasibility to capture and detect ringing in the differential phase current. Determining frequency characteristics of the current ringing and its relation with aging could enable a diagnostic system integrated with existing hardware resources from the power system, mainly the power inverter. In order to apply the wideband AC current sensor, a power drive test system was implemented. The test system included a brushless DC motor along with a high voltage inverter. The power inverter contains a typical six Insulated Gate Bipolar Transistor (IGBT) configuration for power inversion. The power module was modified to allow easy replacement of healthy IGBTs with aged IGBTs to evaluate the changes in the ringing characteristics, indicative of device aging. A thermo-electrical methodology was employed to age the IGBTs; this methodology is applicable to other power semiconductors as well. This paper establishes the feasibility of applying wideband differential AC current sensors to detect current ringing and its characterization for detecting power semiconductor aging.

As "more electrical" technologies become prevalent in the aeronautical and aerospace systems, the need to develop innovative monitoring, diagnostic and fault tolerant techniques for electrical systems is becoming more

978-1-4577-0557-1/12/$26.00 ©2012 IEEE

important.

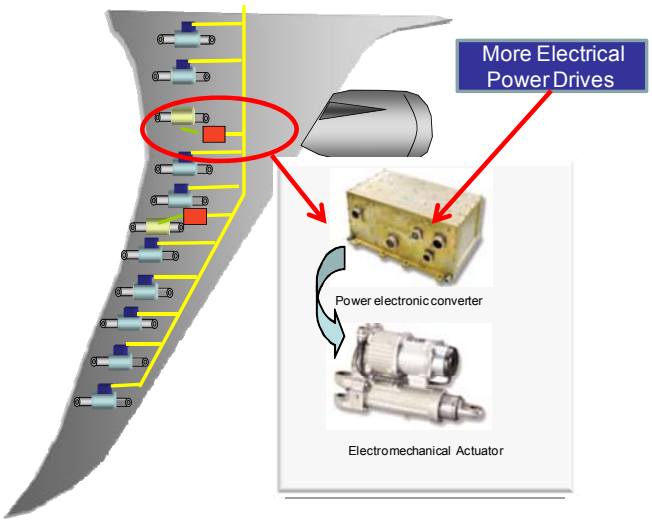

Figure 1 - "More electrical aircraft" with significantly more power drives

2. RINGING CHARACTERIZATION PRINCIPLES

The step inputs introduced by the PWM waveform in a power drive system elicit a response in the system. The system's response at high frequencies establishes the ringing. High frequency responses (>1MHz) in power drives are mainly attributed to small internal or parasitic capacitances, inductances, and resistances that are part of the intrinsic models of each of the components in the power drive system. When subjected to step inputs, these parasitic or internal elements interact with each other and produce ringing. As these power components deteriorate over time, their internal parasitic elements also age. Since high frequency responses are dependent on parasitic elements, a change in ringing is expected with component aging. Based on this, we can consider if ringing characterization could be used to measure the relative aging effects in power components such as switching transistors, diodes, and stator motor windings.

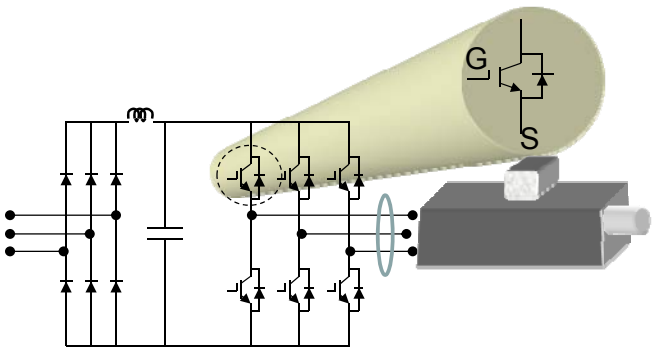

Figure 2 - Application of ringing characterization

Ringing characterization technique [1-3] can be integrated with existing hardware resources from the power system, mainly the power inverter, which contains a microprocessor and sensors that already measure voltages and currents throughout the system. Resources from the microprocessor are utilized during free available microcontroller time to perform data acquisition, feature calculation, and fault detection. A diagram illustrating how the ringing characterization technique can be integrated into an existing power system is provided in Figure 2.

Simplified Modeling

Assuming the ringing characterization is correlated to the component aging effects, the relative aging effects of the power electric drive switching transistors can be derived by extracting the ringing from the motor phase current. The equivalent circuit model formed by the drive, switching transistor, and motor is modeled as a second order system. The circuit model is formed by using the capacitance and inductance of the switching device in conjunction with the inductance and resistance of the motor stator winding; the inductance of the stator winding behaves as a current source. Major contributors to the frequency response of the circuit are the parasitic capacitances and inductances present in the semiconductor and motor windings. Defects/errors in the fabrication process have shown to lead to variability in semiconductor capacitances [6-13]. Similar relationships are also observed for motor windings [4,5].

During a transition between off-to-on states for a transistor such as an IGBT, the drain-to-source properties may be modeled as a switched capacitor for a short period of time. During this transition, second and third order harmonic oscillations are observed between the inductive load of the motor and the non-linear capacitive behavior of the semiconductor. Figure 3 illustrates a simplified series model of the ringing oscillation observed during the transition between transistor (S1) and its clamping diode (S2). This transition is observed as a step response of a second order system. The circuit model of the phenomena includes the two switches (S1 & S2) and the stator-winding coil of the circuit as shown in Figure 3(b). Figure 3(c) shows a simplified characterization of the system as a step response of a second order circuit.

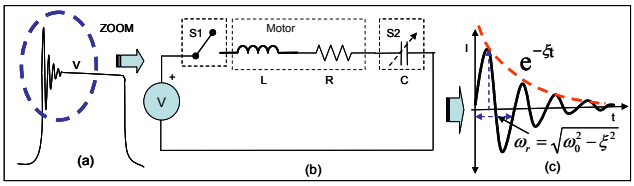

Figure 3 - Modeling ringing characterization as a second order system

The RLC system illustrated in Figure 3(b) can be expressed by a second-order differential equation as shown below in Equation 1.

$$\frac{\partial^2 i(t)}{\partial t^2} + 2\xi \frac{\partial i(t)}{\partial t} + \omega_o^2 \mathrm{i}(t) = 0 \qquad (1)$$

Expressions for the damping factor and resonant frequency, defined in units of [rad/s], are also provided in Equations 2 and 3 accordingly.

978-1-4577-0557-1/12/$26.00 ©2012 IEEE

$$\xi = \frac{R}{2L} \quad (2)$$

$$\omega_o = \frac{1}{\sqrt{LC}} \quad (3)$$

The current modeled in Equation 1 exhibits an oscillatory behavior as shown earlier in Figure 3 (a). The solution of differential Equation (1) leads to the expression for the current provided in Equation 4.

$$i(t) = e^{-\xi t}\left[A_1 e^{\sqrt{\xi^2-\omega_0^2}} + A_1 e^{\sqrt{\xi^2-\omega_0^2}}\right] \quad (4)$$

When the damping factor is less than the resonant frequency, the solution becomes complex creating the ringing oscillation. The resulting expression is provided below in Equation 5, where the ringing frequency, expressed in [rad/s], is defined in Equation 6.

$$i(t) = e^{-\xi t}\left[be^{j\omega_r}\right] \quad (5)$$

$$\omega_r = \sqrt{\omega_0^2 - \xi^2} \quad (6)$$

The final expression for the current given in Equation 5, represents the harmonic frequency of the voltage waveform shown earlier in Figure 3(a). Measuring this quantity provides the opportunity to track on-line values of the power device parameters, such as the damping factor, voltage overshoot, and ringing resonant frequency, which may be used as precursors to failure.

Shunt Model

The RLC system in parallel or shunt configuration can be expressed as a second-order differential equation as shown below in Equation 7

$$\frac{\partial^2 v(t)}{\partial t^2} + 2\xi\frac{\partial v(t)}{\partial t} + \omega_o^2 v(t) = 0 \quad (7)$$

$$\xi = \frac{1}{2RC} \quad (8)$$

$$\omega_o = \frac{1}{\sqrt{LC}} \quad (9)$$

where Equation 8 and 9 represent the damping factor and resonant frequency, respectively.

A general solution to the differential equation, presented in Equation 10, has a similar form to the solution for current.

$$v(t) = e^{-\xi t}\left[B_1 e^{\sqrt{\xi^2-\omega_0^2}} + B_2 e^{\sqrt{\xi^2-\omega_0^2}}\right] \quad (10)$$

3. Aged IGBT Diagnostic By Ringing Characterization

In the previous section, ringing was identified and characterized in healthy components. In order to analyze the effects of aging on IGBT ringing, a testing methodology was developed to induce permanent degradation while preserving device operability. To achieve this, a control system was used to induce transistor accelerated degradation by operating it at high temperature. Both front and back case temperature, $T_{case(f)}$, and $T_{case(b)}$, gate-to-emitter voltage, V_{GE}, collector -to-emitter voltage, V_{DS}, collector current, I_C, and gate current, I_G, were monitored to regulate a PWM signal applied to the transistor gate. In addition, a power supply was connected between the drain and source of the IGBT.

Accelerated Aging System

Accelerated aging was performed on IGBTs using the aging system shown in Figure 4. During the aging process, the transistor's case temperature was controlled in a feedback loop to provide gradual regulation of the aging process (damage accumulation). The process was accelerated by removing the heat sink from the transistor in order to elevate the junction temperature at a lower operating current, I_D. The temperature was measured along the front and back surfaces of the power semiconductor to approximate the junction temperature of the device, T_j using the thermal model of the power device and thermal resistance values provided by the manufacturer. A data acquisition system was used to measure $T_{case(f)}$, $T_{case(b)}$, V_{GE}, V_{CE}, I_C, and I_G to control the PWM signal applied to the IGBT. The PWM sequence was determined based on estimating the junction temperature of the IGBT in real-time. A temperature set point was established at 125% of the maximum operational junction temperature defined by the manufacturer. Then, IGBTs were aged by thermo-electrical stress until latching was observed; experimental data indicated this event occurs after observing a gradual increase in I_G. Once latching occurred, the transistors were turned off for several minutes. After this recovery period, several transistors retained full operational capabilities with non-observable changes in the nominal operating parameters V_{DS}, I_D, V_{GS}, and I_G. Subsequent latching events typically occurred at 5°C below the preceding latching event. Also, the time between latching events decreased with the number of latching events observed. The occurrence of secondary latching at lower temperature, in a shorter time period and at the same current is an indication of an incipient fault attributed to device degradation. Finally, test boards were fabricated, identical to those shown in Figure 4(b) to facilitate rapid aging of multiple transistors and validate the experimental results.

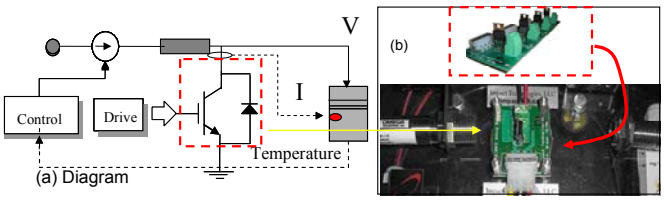

Figure 4 - (a) Diagram of the thermo-electrical accelerated aging system; (b) IGBT test board and aging system

Effect of Aging in Ringing Signature

The ringing signatures from aged, or degraded transistors, were evaluated for a power drive system. A power drive evaluation test-bed was developed to evaluate the ringing effects in a controlled environment. The correspondence between components of the standard system (denoted by

978-1-4577-0557-1/12/$26.00 ©2012 IEEE

dashed rectangles) and the ringing evaluation test-bed is shown in Figure 5. The simplified diagram shown in Figure 5(b) identifies the three main components used to study the effects of ringing in power drives, a single-phase of the three-phase motor winding, a free-wheeling diode, and an IGBT transistor. Figure 5(c) details the main parametric elements of the power devices involved in the switching.

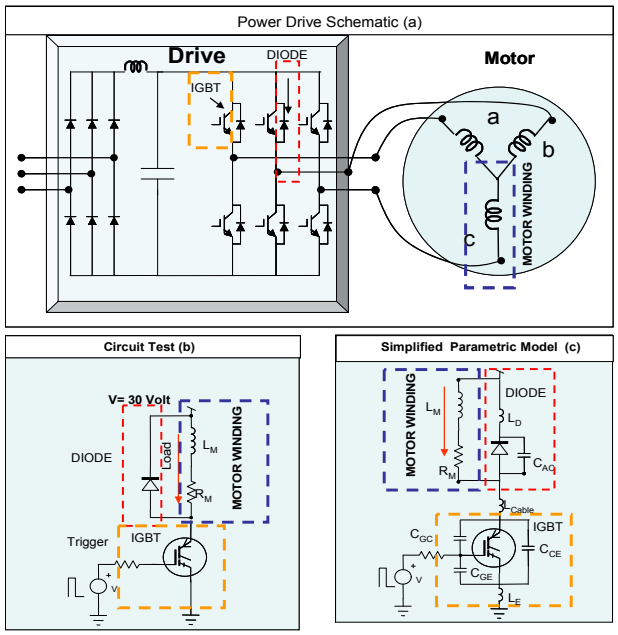

Figure 5 - (a) Power drive, (b) corresponding evaluation test-bed, and (c) transistor model

The IGBT is typically modeled with the three terminal capacitances C_{GE}, C_{GC}, C_{CE} , and one parasitic inductance-capacitance (L_E). For the diode only two parametric components are highlighted, the Cathode-Anode capacitance (C_{AC}) and the parasitic diode inductance (L_D). The motor is represented by its stator inductance and resistance. Note, the winding capacitance and coil ground capacitance are omitted since the main interest is the power device.

The transistors were evaluated during both healthy and aged stages to study ringing characteristics observed during normal inverter operation. Three transistor devices were compared using the ringing characterization technique presented in Section 2. Figure 6 identifies the changes in the dynamic behavior of the IGBT switching properties before (top) and after aging (bottom). The blue signals correspond to the device current. An appreciable increase in the damping coefficient, ξ, and attenuation in ringing at high frequencies were observed for all three transistors after aging.

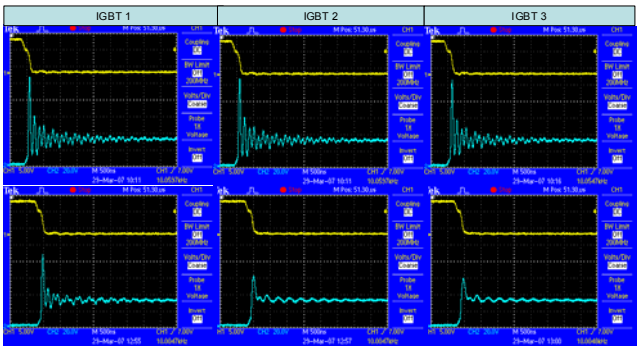

Figure 6 - Changes in the ringing characteristic of new (top) vs. aged (bottom) IGBTs for three transistors

Further ringing comparisons between a new transistor (T1) and three aged transistors (T2, T3, and T4) in different stages of degradation are provided in Figure 7.

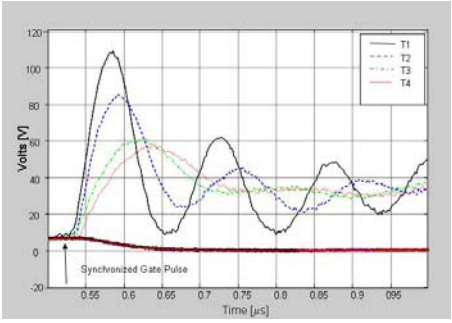

Figure 7 - Changes in the ringing characteristic of new (T1) vs. aged (T2, T3, and T4) IGBTs

The aged states correspond to the number of latch events each transistor was subjected to before evaluation. Transistors T1 through T4 were subjected to 0 through 3 latch events, respectively. In addition, Figure 7 illustrates the increase of damping (ζ) with aging. An increase is also observed in the first oscillation period of the ringing as the aging increases from transistors T1 through T4. Considering the simplified ringing model, depicted earlier in Figure 5, the results observed in Figure 7 suggest an increase in the equivalent dynamic resistance and a reduction in the equivalent dynamic capacitance of the IGBT. This suggests the inductance of the simplified ringing remains constant after transistor aging occurs. Note that the waveforms were aligned using the gate pulse waveform as a triggering or reference sequence.

Although changes in the ringing characteristic are evident, further analysis is required to identify specific frequency changes in the ringing signal to design a practical diagnostic sensor capable of detecting transistor aging. After signal processing, Figure 9 shows the primary and secondary ringing frequencies at 2 MHz and 5 MHz, respectively. In order to obtain each frequency, a transform was applied to the original signal, using the inverse exponential curve fitted to the damping envelope as shown in Figure 8. The resulting signal contained the non-attenuated frequencies of the ringing characteristic. With the non-damped frequency response the attenuation of the primary and secondary frequency components can be tracked.

978-1-4577-0557-1/12/$26.00 ©2012 IEEE

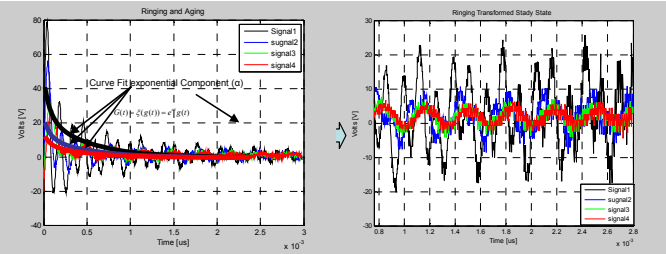

Figure 8 - Undamping current transformation from oscillating exponential to oscillating signal for frequency analysis

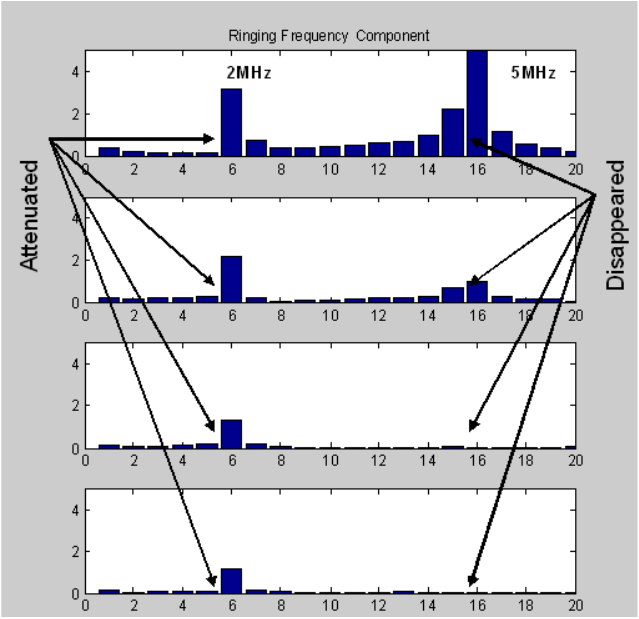

Figure 9 - Ringing frequency content attenuation

4. TEST BENCH

General Description

Figure 10 shows the experimental architecture implemented in the test bench shown in Figure 11. The brushless DC (BLDC) class B actuator shown in the setup is AB23003 and the motor parameters are listed in Table 1. The 3-phase power inverter is the Microchip™ dsPICDEM™ High Voltage Power Module where the motor controller is the Microchip™ dsPICDEM™ MC1 Motor Control Development Board. The hysteresis brake used to simulate the load on the actuator is Magtrol™ HB-700 with 600 mA rated current and 2.8 Nm rated torque at the rated current. The laptop computer runs a graphical user interface (GUI) that allows for quick customization of actuator operational profile including speed and load settings.

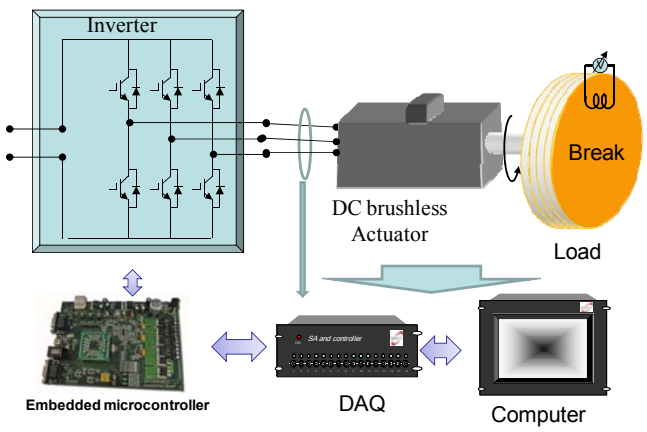

Figure 10 - Test bench architecture

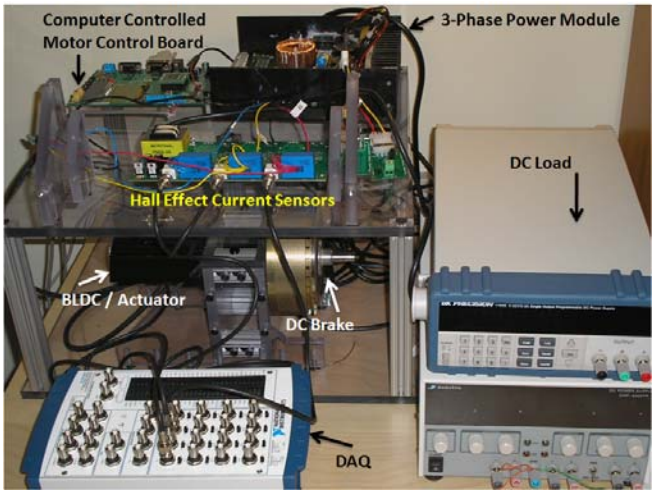

Figure 11: Test bench implementation

Table 1 - Actuator parameters

Nominal Power: 179W (0.24 HP)	
Rs	9.16 Ohms
Ls	7.68 mH
Interia	0.158 kg-cm²
Pole Pairs	1
Rth	1.7 °C/Watt

Sensor and Conditioning Hardware

The differential current sensor was implemented using an in-house signal conditioning board based on the Hall effect and a wideband low cost sensor as shown in Figure 12. The wideband sensor shown on the right side of the figure is assembled using wires wound around a ferrous toroid. The wideband sensor allows detection of high frequency components of current signals.

978-1-4577-0557-1/12/$26.00 ©2012 IEEE

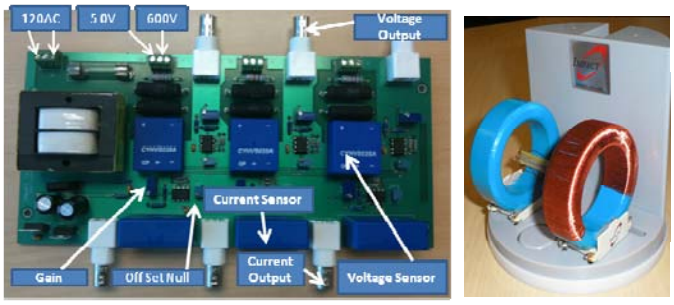

Figure 12 - a) Signal conditioning board b) Wideband current sensor

5. EXPERIMENTAL RESULTS

Ringing Comparison

Figure 13 below shows the results of the current signals captured using different current sensors. The blue signal represents the current in Phase B of the actuator using the COTS current sensor on Impact's general instrumentation board. The purple signal represents the current signal captured directly from the motor control development board for Phase B. Finally, the green signal represents the cumulative leakage current for all three phases of the actuator using the sensor that Impact is developing, as shown in Figure 12. The signals were triggered using the high side transistor signal for Phase B. It can be seen that there are ringing components present in the current signals but the ringing characteristics are influenced by the sensor type.

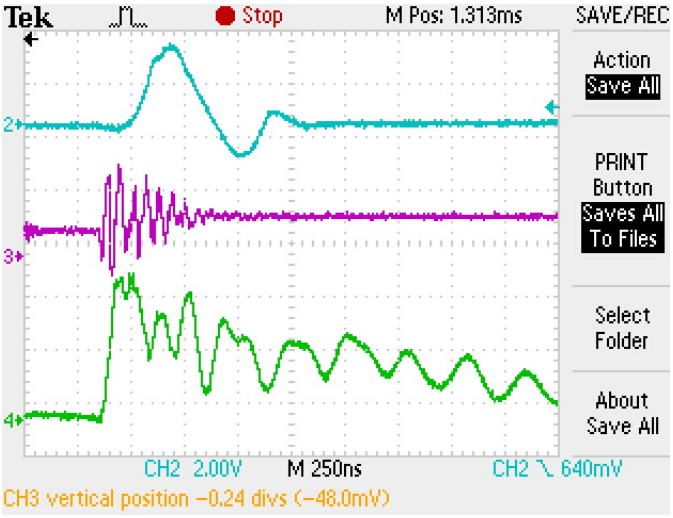

Figure 13 - Actuator test bench ringing signals

Detecting IGBT Aging Using Wideband AC Current Sensor

The two figures below show the FFT analysis of the current ringing signal captured using the wideband AC leakage current sensor being developed by Impact and described in previous sections. Using the test bench shown in Figure 11, eight samples of the current ringing with all three phases of the actuator current through the current sensor. The test was conducted for the power drive system with all six healthy IGBTs and repeated with 5 healthy and 1 aged IGBT in the power module. The aged IGBT was thermo-electrically aged using the technique described in section 3. Figure 14 shows the normalized FFT of the current signals captured using the wideband AC current sensor on the test bench with all healthy IGBTs. The horizontal axis represents the frequency and vertical axis represents the magnitude of the FFT. Figure 15 shows the normalized FFT of the current signals captured using the same wideband AC current sensor with the otherwise identical test bench with 5 healthy IGBTs and one aged IGBT. It should be noted that both figures are plotted on the same vertical scale to provide easy comparison in the frequency response for the two scenarios. It is clear that the frequency response is lower in the aged IGBT data set as expected for aged devices. These preliminary results establish the feasibility of using a wideband AC current sensor to detect semiconductor aging in power drive systems.

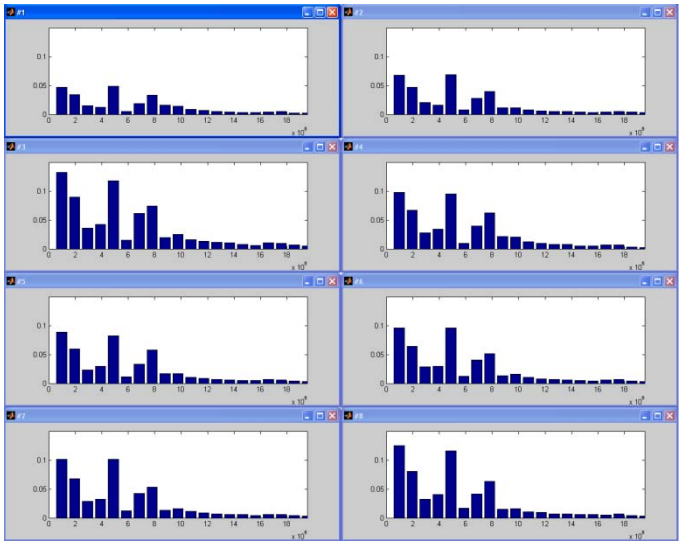

Figure 14 - FFT analysis of the current ringing signals with healthy IGBT

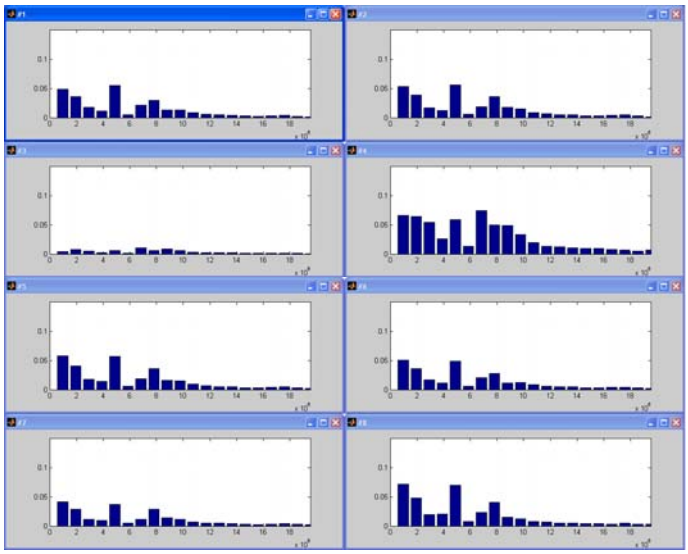

Figure 15 - FFT analysis of the current ringing signals with aged IGBT

978-1-4577-0557-1/12/$26.00 ©2012 IEEE

The above results were based on an experiment that was conducted using the experimental test bench and current signals were acquired using the wideband AC current sensor. The sensor was placed around all three phase currents. The next phase of testing modified the test methodology with the current sensor was isolated to include just the external module containing the replaceable IGBT. The test methodology was similar to the preceding phase. Current ringing signals were acquired using a healthy IGBT plugged in the replaceable transistor board for the modified power module. Next, the healthy IGBT was replaced with a previously aged IGBT and current ringing was acquired again. In both scenarios, the test bench was operated under similar conditions with the actuator operating at full speed and the DC brake connected to the programmable power supply to simulate load conditions. Ten sets of data were acquired using a high speed oscilloscope and frequency analysis was conducted. Figures below highlight the results from the testing.

Figure 16 shows the FFT analysis for the current ringing data captured for system with all healthy IGBTs. As mentioned in the previous paragraph, this ringing data was captured for only the current associated to the IGBT which will be replaced with an aged one in the next test.

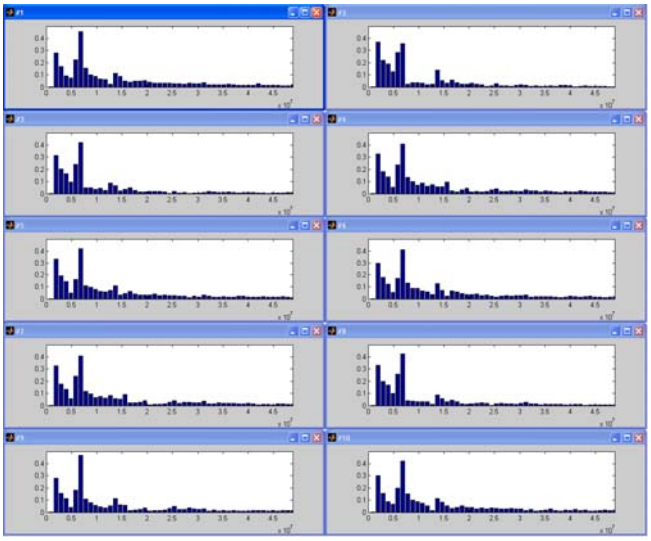

Figure 16 - FFT analysis of healthy IGBT ringing in operating test bench

Next, the healthy IGBT in the modified power module was replaced with a previously aged IGBT and ringing current signals were acquired using the same test procedures. Figure 17 shows the FFT of the aged IGBT current ringing.

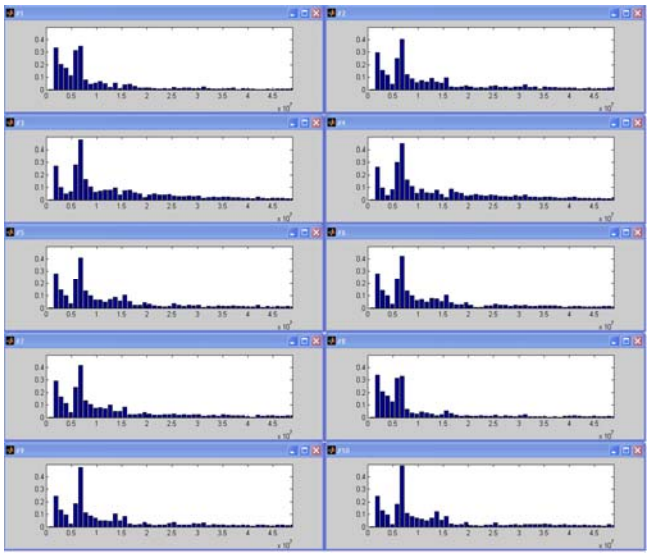

Figure 17 - FFT analysis of aged IGBT ringing in operating test bench system

Based on the results shown in Figure 16 and Figure 17, a comparison was done on the two test results to detect aging effects in the current ringing FFT analysis. Figure 18 shows the average frequency response for the ten data sets that were acquired for healthy and aged IGBT current ringing. For each frequency, it also shows the standard deviation of the frequency response. It should be noted that as power semiconductor devices age, their frequency response for certain frequencies attenuates. As can be seen, the frequency content seems to be attenuating in the lower end of the spectrum, specifically 1-4 MHz range. However, these results do not show the changes in the frequency response conclusively. Moreover, these results were achieved using an IGBT device that was aged several months ago. Therefore, additional testing needs to be done for more detailed characterization.

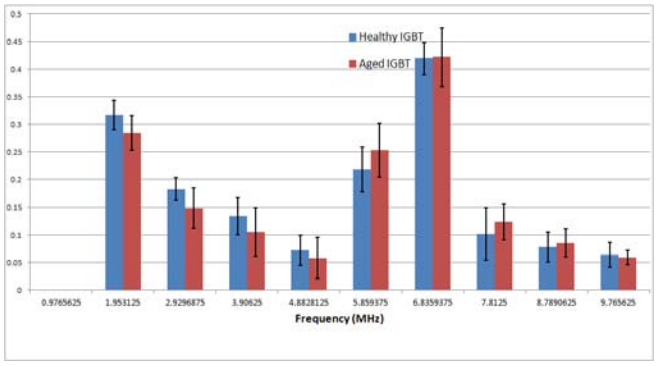

Figure 18 - Average FFT with standard deviation comparing healthy and aged IGBTs

6. CONCLUSION

In this paper we established the feasibility of detecting power semiconductor device aging using a wideband differential AC current sensor. The preliminary results presented in this paper show that device parameters change due to the aging effects, which is reflected in the attenuated

978-1-4577-0557-1/12/$26.00 ©2012 IEEE

frequency response. Further work is needed to do a detailed characterization of device aging and corresponding frequency attenuation from the healthy stage to the point of failure. The results presented here provide a promising technique that, with further development, could lead to a compact sensor capable of detecting power semiconductor aging. Early detection promises less downtime through the application of fault tolerant techniques to avoid a complete system failure.

ACKNOWLEDGEMENT

This work was funded by NASA SBIR program, with oversight and technical support provided by NASA Ames Research Center.

REFERENCES

[1] M. A. Rodríguez1, A.Claudio , D. Theilliol, and L. G. Vela "A New Fault Detection Technique for IGBT Based on Gate Voltage Monitoring" PESC 2007, pp. 1000-1005

[2] A.E. Ginart, D Brown, PW Kalgren, MJ Roemer "On-line Ringing Characterization as a Diagnostic Technique for IGBTs in Power Drives" accepted for publication on IEEE TRANS on Instrumentation, & Measurement

[3] A.E. Ginart, D Brown, PW Kalgren, MJ Roemer "On-line Ringing Characterization as a PHM Technique for Power Drives and Electrical Machinery", IEEE Autotestcon, Sept. 2007, pp. 654-659.

[4] G. Stone, E.A. Boulter, I. Culbert, and H. Dhirani "Electrical Insulation for Rotating Machines". Institute of Electrical and Electronics Engineers, 2004

[5] IEEE 522-1992, "Guide for Testing Turn-to-Turn Insulation on Form Wound Stator Coils for Alternating Current Rotating Electrical Machines."

[6] D.K Scroder, "Semiconductor Material and Device Characterization", John Wiley and Sons, New York, 1990

[7] P. Srinivasan, "Reliability of Solder Die Attaches for High Power Application," Master's thesis, Dept. Mech. Eng., Univ. Maryland, College Park, MD, 2000.

[8] D.C. Katsis "Thermal Characterization of Die-Attach Degradation in the Power MOSFET" PhD thesis Virginia Polytechnic Institute, 2003.

[9] W. Wu, G. Gao, L. Dong, Z. Wang, M. Held, P. Jacob, P. Scacco, "Thermal Reliability of Power Insulated Gate Bipolar Transistor IGBT) Modules," 12thAnnual IEEE Semiconductor Thermal Measurement and Management Symposium, 1996.

[10] D.C. Katsis, J.D. van Wyk, "Void-induced thermal impedance in power semiconductor modules: some transient temperature effects" IEEE Transactions on Industry Applications,Sept.-Oct. 2003,Vol.39, No 5, pp.1239- 1246

[11] Miranda, E. and Sune´, J. , "Electron transport through broken down ultra-thin SiO2 layers in MOS devices", Microelectronics Reliability, Vol. 44, pp. 1-23. 2004.

[12] A. Feinberg, P. Ersland, V. Kaper, and A. Widom, "On aging of key transistor device parameters," in Proc. Inst. Environmental Sciences & Technology, 2000, pp. 231–236.

[13] A.A. Feinberg, A. Widom. "On Thermodynamic Reliability Engineering." IEEE TRANSACTIONS ON RELIABILITY, VOL. 49, NO. 2, JUNE 2000.

BIOGRAPHIES

Irfan N. Ali *is a Project Engineer at Impact Technologies. He received a B.S. and M.S. in Electrical Engineering from Georgia Institute of Technology in 2007 and 2009 respectively. He has been a part of the Impact Technologies team developing innovative technologies for electronic system health assessment since joining. He has worked intimately over the past year with the research and development of the power device PHM technology. On the technical side he has developed algorithms, test plans and automated test benches in support of software and hardware product development. On the programmatic side he has led SBIR and commercial efforts in the health management areas of power supplies, industrial systems, and avionic data and systems.*

Antonio E. Ginart *(S'89–M'01–SM'07) Received the B.Sc. and M Sc degrees in Electrical Engineering from Simon Bolivar University , Caracas, Venezuela in 1986 and 1990, respectively, and the Ph.D. in Electrical Engineering from the Georgia Institute of Technology in 2001. He has over 20 years of experience in motors, electronic drives, and industrial controls. He was an Instructor, Assistant Professor, and later Associate Professor at Simon Bolivar University from 1989 to 2002. He was a consultant for Aureal Semiconductors, Inc. in power amplification from 1999 to 2000, where he pioneered the effort to develop Class AD amplifiers. At Impact Technologies, he is responsible of developing intelligent automated monitoring systems for electrical and electronics equipment for industrial and military applications. His research has led to over 50 publications.*

Jonathan W. Goldin *is Senior Project Engineer at Impact Technologies, LLC. In his 5 years at Impact Technologies, he has worked on a wide array of projects. He is experienced in developing agent-based software that can predict and schedule maintenance to minimize downtime. Embedded systems are also an interest. He has worked on a several embedded platforms, including Impact's sensor mote used in Impact's eSPAN and Missile Monitor programs. Jonathan also has hands-on skills used to design, build and test hardware. He is an alumnus of Georgia Institute of Technology, earning a B.S. degree in Electrical Engineering in 2005.*

Patrick W. Kalgren *has a B.S. degree in Computer Engineering from Penn State University and manages the Electronic Systems PHM group at Impact Technologies, leading the development of improved diagnostics and failure prediction to enable health management for electronic systems. Patrick has a 20+year background in mechanical and electronic system analysis, diagnosis and repair. While previously employed by PSU ARL, Patrick researched automated classifiers and developed performance tests to assess cross data type performance. At Impact, he has developed advanced signal processing, applied AI techniques to fault classification, researched advanced database design and supervised various software projects related to vehicle health management. Patrick is a member of Tau Beta Pi, IEEE, The IEEE Standards Association, and the IEEE Computer Society.*

Michael J. Roemer *received his Bachelor of Science degree in Electrical Engineering and his Doctorate in Mechanical Engineering from the State University of New York at Buffalo. He is the co-founder and Director of Engineering at Impact Technologies with over 18 years experience in the*

978-1-4577-0557-1/12/$26.00 ©2012 IEEE

development of real-time, monitoring, diagnostic and prognostic systems for a wide range of military and commercial applications. He has extensive working knowledge in technologies such as artificial intelligence methods, vibration analysis, electrical signal analysis, aero-thermal performance monitoring, non-destructive structural evaluation and monitoring, and probabilistic risk assessment methods. Dr. Roemer is a past Chairman of the Machinery Failure Prevention Technology (MFPT) Society, Prognostic Lead for the SAE E-32 Engine Condition Monitoring Committee, Member of the IGTI Marine committee and ASME Controls and Diagnostics Committee and Adjunct Professor of Mechanical Engineering at the Rochester Institute of Technology. He is the co-author of a recent book published by Wiley titled "Intelligent Fault Diagnosis and Prognosis for Engineering Systems" and has written or co-authored more than 100 technical papers related to integrated systems health management.

Scott Poll *received the B.S.E. degree in Aerospace Engineering from the University of Michigan, Ann Arbor, in 1994, and the M.S. degree in Aeronautical Engineering from the California Institute of Technology, Pasadena, in 1995. He is currently a Research Engineer with the National Aeronautics and Space Administration (NASA) Ames Research Center, Moffett Field, CA, where he is the deputy lead for the Diagnostics and Prognostics Group in the Intelligent Systems Division. He is co-leading the evolution of a laboratory designed to enable the development, maturation, and benchmarking of diagnostic, prognostic, and decision technologies for system health management applications. He was previously the Associate Principal Investigator for Prognostics in the Integrated Vehicle Health Management Project in NASA's Aviation Safety Program.*

978-1-4577-0557-1/12/$26.00 ©2012 IEEE